



1 **Effect of boundary layer low-level jet on fog fast spatial propagation**

2 Shuqi Yan¹, Hongbin Wang^{1,*}, Xiaohui Liu², Fan Zu¹, Duanyang Liu^{1,*}

3 ¹Key Laboratory of Transportation Meteorology of China Meteorological Administration, Nanjing Joint Institute for Atmospheric
4 Sciences, Nanjing, 210041, China

5 ²Merchant Marine College, Shanghai Maritime University, Shanghai, 201306, China

6
7 *Correspondence to:* Hongbin Wang (kaihren@163.com); Duanyang Liu (liuduanyang2001@126.com)

8 **Abstract.** The spatiotemporal variation of fog reflects the complex interactions among fog, boundary layer thermodynam-
9 ics and synoptic systems. Previous studies revealed that fog can present **fast spatial propagation** feature and attribute it to
10 boundary layer low-level jet (BLLJ), but the effect of BLLJ on fog propagation is not quantitatively understood. Here we
11 analyze a large-scale fog event in Jiangsu, China from 20 to 21 January 2020. Satellite retrievals show that fog propagates
12 from southeast coastal area to northwest inland with the speed of 9.6 m/s, which is three times larger than the ground wind
13 speeds. The ground meteorologies are insufficient to explain the fog fast propagation, which is further investigated by
14 WRF simulations. The fog fast propagation could be attributed to the BLLJ occurring between 50 and 500 m, because the
15 wind speeds (10 m/s) and directions (southeast) of BLLJ core are consistent with fog propagation. Through sensitive ex-
16 periments and process analysis, three possible mechanisms of BLLJ are revealed: 1) The abundant oceanic moisture is
17 transported inland, increasing the humidity of boundary layer and promoting condensation; 2) The oceanic warm air is
18 transported inland, enhancing the inversion layer and favouring moisture accumulation; 3) The moisture advection proba-
19 bly promotes upper-level fog formation, and later it subsides to ground by turbulent mixing of fog droplets. The fog prop-
20 agation speed would decrease notably by 6.4m/s (66%) if the BLLJ-related moisture and warm advections are turned off.

21 **1. Introduction**

22 Fog is a kind of low-visibility weather phenomenon that occurs at near surface, causing adverse impacts on traffic trans-
23 portation. The formation, development and dissipation of fog are the comprehensive results of the interactions among radi-
24 ation, moisture, microphysics, turbulence, aerosols and other factors (Gultepe et al., 2007; Koračín et al., 2014; Nakanishi,
25 2000). The relations of fog with meteorological factors are highly variable under different conditions. Therefore, the
26 mechanism of fog evolution needs to be intensively studied.

27 Under favourable conditions, the fog intensity or its spatial extent can develop extraordinarily fast with time. Field obser-
28 vations conducted at single site reveal that visibility in fog can deteriorate drastically, from about 1km to less than 200m
29 within 30min (Li et al., 2019). It is referred to as fog burst reinforcement, which is firstly raised by Korb et al. (1970) and
30 systematically reviewed by Liu et al. (2012) and Li et al. (2019). Fog burst reinforcement is accompanied by the drastic
31 formation of fog droplets, sudden increase of fog liquid water and broadening of droplet spectrum (Liu et al., 2017; Liu et
32 al., 2021). Additionally, fog can develop rather fast in spatial extent, i.e., the **fast spatial propagation of fog** (Zhu et al.,
33 2022). It is reflected by the successive visibility dropping in space along a certain direction. The influencing factors of fast



34 spatial propagation could be more complex than that of the burst reinforcement at single site, which have received fewer
35 quantitative studies recently.

36 Synoptic systems and planetary boundary layer (PBL) thermodynamic structures are key to understanding the cause of fog
37 burst reinforcement and fast propagation. Weak cold air invasion and radiative cooling is an important factor for fog burst
38 reinforcement and fast propagation (Liu et al., 2011; Wang et al., 2020). Dhangar et al. (2021) demonstrated that the radiative
39 cooling at surface and fog top can increase supersaturation and promote fog vertical development. Shen et al. (2022)
40 found that the different cooling rates at two nearby stations lead to a remarkable difference in fog formation time, fog du-
41 ration and vertical extent. Sufficient water supply is also an important factor. Wobrock et al. (1992) revealed that the role
42 of moisture advection outweighs radiative cooling in large-scale fog events. Pu et al. (2008) found that two layers of mois-
43 ture advection enhance fog development and maintenance. Under stable synoptic systems, the PBL thermodynamic can
44 also favour fog burst reinforcement and fast fog propagation. The formation of dense fog is usually accompanied by strong
45 inversion layer, of which the intensity could reach 16K/100m (Pu et al., 2008; Liu et al., 2012). Liu et al. (2016) found that
46 upper-level warm advection and low-level cold advection significantly enhance inversion intensity and promote fog de-
47 velopment. The vapor advection resulting from southerly winds further increases fog intensity. Appropriate turbulence also
48 facilitates fog formation and enhancement (Ye et al., 2015). Turbulent results in the exchange of heat and moisture within
49 PBL, e.g., the downward entrainment of vapor and cold air can promote condensation and droplet formation (Liu et al.,
50 2016; Zhang et al., 2005). Other studies highlight the role of hygroscopic aerosols and aerosol indirect effects in strong fog
51 events (e.g., Boutle et al., 2017; Quan et al., 2021; Wang et al., 2023; Yan et al., 2021).

52 Previous studies find that the large-scale fog events are accompanied by boundary layer low-level jet (BLLJ), and try to
53 attribute the spatial propagation of fog to BLLJ. The causes of BLLJ include such as synoptic systems, terrain effect and
54 inertial oscillation (Kraus et al., 1985). Tian et al. (2019) demonstrated that the warm-and-wet southerly BLLJ favours wa-
55 ter vapor transportation and inversion layer construction, and later the fog is triggered by a weak cold front invasion. Wu et
56 al. (2020) found that strong northerly BLLJ associated with cold air can destroy inversion layer and lead to early dissipa-
57 tion of fog, while weak BLLJ can promote fog maintenance. Li et al. (2012) revealed that the strengthened turbulence gener-
58 ated by BLLJ wind shear promotes vertical mixing and facilitates fog development. However, the relations between
59 BLLJ and fog propagation and the key synoptic factors have not been quantitatively addressed. Also, the current horizontal
60 and vertical observations are not sufficient to reveal the mechanism of fog propagation. It requires further investigation by
61 numerical models.

62 In this work, we study a large-scale fog event with fast propagation feature occurring in Jiangsu Province, China from 20
63 to 21 January 2020. By combination of observations and numerical simulations, we aim to quantitatively reveal the BLLJ
64 effect on fast fog propagation to and identify the key impact factors and mechanisms. This work is expected to better un-
65 derstand the complex interactions among synoptic systems, PBL thermodynamics and fog spatial propagation, as well as
66 provide prediction indicators for operational fog forecast. The study is organized as follows: Section 2 describes the data,
67 methods and numerical models of this study. Sections 3.1 to 3.4 analyze the fog propagation feature and PBL characteris-
68 tics. Section 3.5 quantitatively study the BLLJ effect on fast fog propagation and identifies key influencing factors. Section
69 4 concludes the findings of this study.



70 **2. Data, methods and model configuration**

71 **2.1 Data and study area**

72 This study focuses on the Jiangsu area, China (Figure 1), where a large-scale fog event occurred from 20 to 21 January
73 2020. We collected the data from 70 ground automatic weather stations (AWS) in Jiangsu Province, China. The data is
74 recorded by every 10 minutes, including visibility, temperature, relative humidity (RH), wind direction and wind speed.
75 This data is used to analyze the temporal variation of meteorology, as well as evaluate the model performance on tempera-
76 ture, RH and wind.

77 The geostationary satellite Himawari 8 (<https://www.eorc.jaxa.jp/tree/index.html>) is used to retrieve nighttime fog area
78 and evaluate the model performance of fog simulation. The high spatiotemporal resolution (2km in space and 1h in time) is
79 suitable for detecting the fast evolution of fog area. This satellite observation includes 16 bands, and the bands at 3.9 and
80 11.2 μm are used.

81 The ERA5 reanalysis data (<https://cds.climate.copernicus.eu/cdsapp#!/dataset/reanalysis-era5-pressure-levels>) is used to
82 analyze synoptic conditions and provide initial & boundary fields for model simulation. The grid resolution is 0.125°
83 (about 12.5km) and the time interval is 6h. All the time in this study is local time (UTC+8).

84 **2.2 Methods**

85 2.2.1 Satellite fog retrieval

86 Since the ground AWS stations are not sufficiently fine in spatial resolution, the high spatiotemporal resolution product of
87 Himawari 8 is suitable to study the propagation of fog. Nighttime fog has notable different optical properties at the bands
88 of 3.9 μm and 11.2 μm , so it can be indicated by the dual-band brightness temperature difference ($T_{bb_{3.9}}$ minus $T_{bb_{11.2}}$)
89 lower than a threshold (Cermak et al., 2008). In this study, the threshold is determined to be -2 K following the dynamic
90 threshold algorithm proposed by Di Vittorio et al. (2002). Daytime fog after 08:00 is not retrieved because we mainly fo-
91 cus on the formation and development stage of fog before 08:00.

92 2.2.2 Fog propagation speed calculation

93 We calculate the propagation speed according to satellite retrieved fog area. At 22:00 on 20 January 2020, a tiny fog area
94 appeared at Nantong and Yanchen coastal region with an area smaller than 50km² (figure not shown). The center of this
95 fog area is set as point A (120.6°E, 32.9°N). We draw a line starting from A with an arbitrary direction, and find its inter-
96 section with the fog boundary area at 07:00 next day (point B). Then the propagation speed in this direction can be calcu-
97 lated by the distance from A to B divided by 9 hours (22:00~07:00). By looping from 0 to 360 with the interval of 1°,
98 propagation speeds in all directions are calculated, and the maximum speed is defined as the fog propagation speed.

99 The fog propagation speed is verified by AWS data. We select three representative stations along the fog propagation di-
100 rection, Dafeng (DF; 120.48°E, 33.20°N, 14m), Baoying (BY; 119.30°E, 33.23°N, 15m), Sihong (SH; 118.22°E, 33.48°N,



101 13m) (Figure 1). According to their distances and the time differences when visibility drops to 200m, the propagation
102 speed between two adjacent stations is calculated.

103 2.2.3 Process analysis on fog

104 The simulated fog is indicated by fog liquid water content (LWC). Process analysis is used to quantify the contribution of
105 each physical process to LWC variation (Schwenkel et al., 2019; Yan et al., 2020). The variation of LWC is related to the
106 following terms:

$$107 \quad \frac{\partial \text{LWC}}{\partial t} = - \underbrace{\left(u \frac{\partial}{\partial x} + v \frac{\partial}{\partial y} + w \frac{\partial}{\partial z} \right)}_{\text{Advc}} \text{LWC} + \left(\frac{\partial \text{LWC}}{\partial t} \right)_{\text{Vmix}} + \left(\frac{\partial \text{LWC}}{\partial t} \right)_{\text{Cond}} + \left(\frac{\partial \text{LWC}}{\partial t} \right)_{\text{Sedi}} + \left(\frac{\partial \text{LWC}}{\partial t} \right)_{\text{other}}$$

108 where Advc includes horizontal and vertical advection, Vmix is associated with the fog droplet vertical exchange by tur-
109 bulent mixing, Cond is the vapor condensation (negative means droplets evaporation), Sedi is fog droplets sedimentation.
110 Other microphysical processes include autoconversion, accretion and cold phase processes. They are much smaller than the
111 previous four processes, so they can be safely ignored.

112 2.3 Model configuration and experiments

113 The Weather Research and Forecasting model (WRF) is implemented to study the fast spatial propagation of fog events.
114 Two domains are set up (Figure 1). The parent domain covers East China, with the grid size of 181×181 and grid interval
115 of 9 km. The nested domain covers Jiangsu Province and its coastal area, with the grid size of 199×199 and grid interval of
116 3 km. To simulate the turbulent process more reasonably, the vertical levels are refined to 42 levels, with 25 levels under
117 1500m and 9 levels under 100m (Yang et al., 2019; Yan et al., 2020). The first model level is about 4m. The model is driv-
118 en by the initial and boundary field from ERA5 Reanalysis. The simulation starts at 08:00 on 19 January and ends at 08:00
119 on 21 January 2020, with the first 24h as spin-up period. All the time in this study is local time (UTC+8).

120 Fog simulation is sensitive to the choice of parameterization schemes (Steenefeld et al., 2014; van der Velde et al., 2010).
121 Through massive tests, the QNSE boundary layer scheme (Sukoriansky et al., 2005) and Pleim-Xiu land surface scheme
122 (Pleim et al., 2009) yield the best simulation performance. Other parameterization schemes are listed in Table 1. The simu-
123 lated fog is indicated by the liquid water content (LWC) greater than 0.015g/kg under the height of 500m, which corre-
124 sponds to horizontal visibility less than 1km (Kunkel, 1983).

125 Apart from the base experiment, three sensitive experiments are performed to elucidate the mechanism of fast fog propa-
126 gation (Table 1). The experiment "Tadv0" turns off the temperature advection within PBL during the fog period. The ex-
127 periment "QvAdv0" and "QcAdv0" are the same as "Tadv0" except that turning off water vapor advection and fog water
128 advection, respectively. The experiment "NoAdv" turns off all the advectons above. Therefore, the differences of the base
129 experiment with Tadv0, QvAdv0, and Qcadv0 represent the effect of temperature advection, moister advection, and fog
130 water advection, respectively. The reasons and results of the sensitive experiments will be discussed in Section 3.5.



131 **3. Results and discussions**

132 **3.1 Fog overview and synoptic background**

133 The studied fog event occurs at the night of 20 January and dissipates in the daytime of 21 January 2020 (Figure 2). Figure
134 3 shows the synoptic situations at 08:00 and 20:00 on 20 January. At 500hpa, a frontal zone is located north of 38°N. The
135 Jiangsu area is dominated by prevailing westerly flows with no obvious troughs. At 850hpa, a ridge moves eastward and
136 controls Jiangsu area. The descending motions associated with the ridge and the nocturnal radiative cooling at ground fa-
137 vour the establishment of inversions. At ground level, a weak cold high pressure moves eastward with the central pressure
138 of 1030hpa. The Jiangsu area is dominated by uniform pressure field with small wind speeds, which strengthens atmos-
139 pheric stratification stability and promotes the accumulation of aerosols and moisture. The moisture condition in Jiangsu is
140 additionally favoured by the water vapor transportation from ocean by easterly winds at 20:00. Under this conductive situ-
141 ation, the fog event occurred from nighttime of 20 to daytime of 21 January over Jiangsu Province (Figure 2).

142 **3.2 Fog and ground meteorology variation**

143 Hourly Himawari 8 satellite image clearly shows the spatial propagation of fog (Figure 2). The fog initials at 22:00 on 20
144 January in Nantong and Yanchen coastal region with an area smaller than 50km². Later, this small fog area expands to a
145 large-scale fog. Specifically, the southeast side of fog area varies relatively slowly, but the northwest side expands re-
146 markably, indicating a large propagation speed. At 07:00 on 21 January, the front of fog expands to Anhui Province. After
147 07:00, the fog begins to dissipate (figure not shown). Figure 4 quantitatively describes the propagation direction and speed
148 of fog. From the east to south directions (the fourth quadrant), fog propagation speed is less than 3m/s. In the
149 west-northwest and west directions, fog propagation speed is larger than 6m/s, and the maximum propagation speed is
150 9.6m/s occurring at 160° direction. The fast propagation of fog is also reported previously in Jiangsu area (Gao et al., 2023;
151 Zhu et al., 2022), where the fog propagates from coastal area to west boundary of Jiangsu within about 10h.

152 Visibilities at three representative stations, Dafeng (DF), Baoying (BY) and Sihong (SH) are used to verify the fog propa-
153 gation speed calculated by satellite (Table 2; Figure 5). At DF, fog forms (visibility less than 1km) early at 19:45 on 20
154 January. The visibility drops sharply at 23:15 and reaches the minimum at about 00:15. At BY and SH, fog forms in turn,
155 and their visibilities also have burst decreasing feature at 03:40 and 07:00, respectively. We calculate the fog propagation
156 speed by the distances among stations and the time differences when visibility drops to 200m. The propagation speed is 7.6
157 m/s between DF and BY and 8.3 m/s between BY and SH. These values correspond to the speed calculated by satellite
158 observation.

159 Figure 5 shows the variation of other meteorological fields. We focus on the characteristics from fog formation to the burst
160 visibility dropping (indicated by yellow dashed lines). At DF, the northerly wind decreases to lower than 1.5m/s at fog
161 formation, which causes the weak cold advection and temperature decreasing. The temperature keeps decreasing and fa-
162 vours the burst reduction of visibility at 23:15. The vapor content (indicated by dew point) increases sharply before 17:00
163 and decreases slightly since then, so the RH increasing after fog formation is caused by temperature drop. At BY and SH,
164 the wind directions are dominantly southeast and the speeds are generally less than 2m/s before fog formation. The tem-



165 perature keeps decreasing and vapor content keeps increasing, leading to the further reduction of visibility. Later, the
166 southeasterly winds obviously enhance by about 1m/s, which may contribute to the burst visibility dropping due to the in-
167 tensified vapor advection from ocean.

168 The preliminary cause of fog formation and intensification are summarized. As located near the ocean, the moisture at DF
169 reaches the maximum prior to fog formation, so the fog formation and intensification are largely caused by radiative cool-
170 ing and weak cold advection. At BY and SH, the temperature cooling rate is weaker than DF, which is partly due to the
171 weak warm advection by southeasterly winds. The vapor advection by southeasterly winds favours fog development, and
172 the burst decrease in visibility coincides with the increase in wind speed. Therefore, deduced from BY and SH, the vapor
173 transportation associated with southeasterly winds could be an important reason for northwesterly propagation of fog.
174 However, it is obvious that the ground wind speed is rather small compared with fog propagation speed. Statistics on AWS
175 stations show that although wind direction (east, southeast and south winds at 70% stations) is generally in accordance
176 with fog propagation direction, wind speed is lower than 3m/s at 97% stations from 22:00 to 07:00, which is about
177 one-third of the fog propagation speed. Therefore, the ground meteorological field is insufficient to explain the fast propa-
178 gation of fog. The fog PBL characteristics and the key influencing factors need to be investigated by numerical simula-
179 tions.

180 3.3 Model evaluation

181 Figure 6 evaluates the model performance on temperature, relative humidity (RH) and wind field at surface. The simulated
182 temperature and RH agree well with observations, with the root mean square error (RMSE) of 1.0K and 11%, respectively.
183 The simulation reasonably captures the wind direction transition from north to east, and the RMSE is less than 1m/s.

184 Figure 2 compares the satellite observed and simulated fog area. The simulation is only evaluated before 07:00, because
185 the dissipation of fog after 08:00 is not the focus in this study. The model reasonably captures the spatiotemporal evolution
186 of fog, with a slight overestimation of 5~10% in fog area.

187 Overall, the simulation reasonably captures the temporal variation of meteorology and reproduces the spatial propagation
188 of fog. It establishes the basis for discerning the mechanism of fog propagation.

189 3.4 Characteristics of fog and PBL structure

190 The thermodynamic variation of PBL is crucial for understanding the propagation of fog. Figure 7a shows the temporal
191 variation of horizontal winds in vertical directions. The simulated wind speed is consistently smaller than 4m/s under about
192 30m, while it remarkably increases with height. At 18:00 on 20 January, a large wind speed zone (>6m/s) forms at the
193 height between 50 and 500m in the east of 120°E. Since then, the large wind zone moves westward quickly accompanied
194 by wind speed increasing. During the fog period, the average wind speed exceeds 6m/s at the height between 50 to 500m
195 (Figure 7b), which is commonly larger than the wind speed in most fog events. Here, we refer to this large wind speed
196 zone as **boundary layer low-level jet (BLLJ)**. The existence of BLLJ is supported by ERA5 reanalysis on 1000hpa and
197 975hpa levels (Figure 7b).



198 The formation of BLLJ is likely caused by the easterly movement of a high pressure at 1000hpa over East China. The cen-
199 tral pressure gets enhanced, which strengthens the pressure gradient over Jiangsu area and favours wind speed increasing
200 (figure not shown). The jet core (maximum wind speed) occurs at about 1000hpa (200m), with the time-averaged speed of
201 10m/s (Figure 7b). At that level, the dominant wind direction is southeast and the wind speed over fog area is 8~16m/s
202 (Figure 7c), which can fit the propagation direction and speed of fog. Also, the expansion speed of vertical fog zone is
203 comparable to the movement speed of jet core (Figure 7a). Therefore, we hypothesize that the southeasterly BLLJ could
204 account for the fast propagation of fog.

205 Previous studies reveal that southerly BLLJ can transport abundant water vapor to China inland and thus promote fog for-
206 mation (Liu et al., 2016; Tian et al., 2019). Figure 8 shows the temporal variation of water vapor mixing ratio (Q_v) profiles.
207 Since the vapor content over the ocean is higher, it is transported to inland areas by southeasterly BLLJ. The BLLJ can
208 further increases the Q_v in PBL by wind speed horizontal convergency and vertical shear. The larger wind speed in BLLJ
209 zone and lower wind speed outside BLLJ zone cause wind speed convergence, which favours the increase in PBL moisture.
210 Additionally, the turbulence generated by vertical shear of wind speed can promote vapor turbulent mixing, leading to the
211 higher Q_v above surface being entrained downward and increasing the ground Q_v (Gao et al., 2007). The Q_v under 300m
212 is generally higher than 3g/kg under the effect of BLLJ. Wu et al. (2020) also found that BLLJ continuously transports
213 water vapor to fog layer, resulting in surface Q_v higher than 3g/kg. It is notable that the expansion of vertical fog area co-
214 incides with the movement of the zone of $Q_v > 4\text{g/kg}$. Therefore, moister advection by BLLJ could be an important reason
215 for fast fog propagation.

216 BLLJ is reported to result in warm advection and deepen inversion layer previously (Tian et al., 2019), and inversion layer
217 is an important reason for fog burst reinforcement in most fog cases (e.g., Li et al., 2019; Liu et al., 2012; Jiao et al., 2016).
218 Figure 9 shows the temporal variation of temperature profile and inversion layer. The inversion layer here refers to the
219 height above ground where temperature monotonically decreases with height. Since 20:00 on 20 January, the ground tem-
220 perature keeps decreasing due to radiative cooling. Within the fog area, the temperature drop is more significant, which is
221 due to the longwave radiative cooling by fog droplets (Bott, 1991; Jia et al., 2018). Approximately above the fog top, there
222 is an obvious warm air mass transported from ocean to inland areas. The BLLJ-induced warm advection increases vertical
223 temperature gradient and strengthens atmospheric stability. Accordingly, the inversion height over non-fog areas basically
224 keeps increasing. The approximate inversion layer height is about 100~300m, with the maximum inversion intensity of
225 15K/100m. Such a strong inversion is also reported in a dense fog event (16K/100m) by Pu et al. (2008). It favours the
226 accumulation of vapor and condensation nuclei, which is also a possible reason for fog formation in the downstream area.

227 Additionally seen from Figure 9, the west boundary of vertical fog region below about 100m has a negative slope, i.e., fog
228 forms at upper level ahead of forming at ground. The height at which fog firstly forms is shown in Figure 10. An initial fog
229 area forms at ground level before 00:00 on 21 January. Since then, the majority of fog area firstly forms at upper level
230 (about 10~66m) over the downstream area, while the ground fog in downstream area forms about 0~20min later than up-
231 per-level fog. The formation of upper-level fog may also be caused by the BLLJ-induced moisture advection. In addition,
232 the fog water advection (Section 2.2.3) to downstream area by BLLJ could also be a potential reason. We hypothesize that
233 the formation of ground fog is partly favoured by the subsidence of upper-level fog. Stratus-lowering or upper-fog subsid-



234 ence to ground has been reported by previous studies (e.g., Haeffelin et al., 2010; Liu et al., 2012); the base height of stratus
235 can be smaller than 100m before fog formation (Dupont et al., 2012; Fathalli et al., 2022), which is basically close to
236 our results (10~66m in Figure 10). While in this event, the upper-fog subsidence remains to be verified by additional
237 high-spatiotemporal resolution vertical observations.

238 According to above results, three potential factors for fog propagation are raised: BLLJ-related temperature advection,
239 moisture advection and fog water advection. These advections possibly promote fog formation in the upper level, and sub-
240 sequently the upper-level fog could subside to ground by the turbulent mixing or sedimentation of fog droplets. Currently,
241 their contributions to fog propagation have not been quantitatively revealed. Therefore, it will be addressed in the next sec-
242 tion.

243 **3.5 Quantitative reasons for fast fog propagation**

244 Four sensitive experiments, Tadv0, QvAdv0, QcAdv0 and NoAdv0 (Section 2.3) are conducted to quantify the respective
245 contributions of temperature advection, moisture advection, fog water advection and all these advections to fog propagation
246 (Figure 11). Under the condition with no advections (Figure 11a-d), there is a 80% decrease in fog area and a 6.4m/s (66%)
247 decrease in propagation speed, which highlights the role of BLLJ-related advections. When turning off temperature advec-
248 tion (Tadv0) (Figure 11e-h), the original fog area in the base experiment shrinks 50% in size and breaks into separate fog
249 patches, and the propagation speed decreases by about 5.2m/s (54%). When turning off moisture advection (QvAdv0)
250 (Figure 11i-l), the fog area shrinks by 62% in size and the propagation speed decreases by about 4.6m/s (48%). When
251 turning off fog water advection (QcAdv0) (Figure 11m-p), the fog area nearly keeps unchanged during 00:00~04:00 and
252 decreases moderately in size (about 25%) at 06:00. The propagation speed decreases moderately by 2.4m/s (25%). Deduced
253 from the changes in fog area and propagation speed under various experiments, we can infer that the BLLJ-related warm
254 and moisture advection, especially moisture advection, could be the major cause of fast spatial propagation, while fog wa-
255 ter advection has a minor contribution.

256 We further perform process analysis on LWC (Section 2.2.3) to illustrate the mechanism of fog propagation (Figure 12).
257 The horizontal and vertical values of Advc and Sedi are at least one order of magnitude smaller than that of Cond and Sedi,
258 indicating that fog water transportation to downstream areas and droplet sedimentation to ground are not the causes of fog
259 propagation. At 00:00 on ground level, Cond is positive over the newly formed fog area (blue and cyan colors surrounding
260 the fog area), indicating that fog firstly forms at ground by radiative cooling before 00:00. After 02:00, Cond is almost
261 negative over the entire fog area, indicating that fog does not firstly form at the ground level (otherwise Cond would have
262 positive values). The formation of ground fog may be contributed by the LWC turbulent entrainment from upper level,
263 because Vmix shows significant positive values after 02:00. In the vertical direction, Vmix and Cond are still two domi-
264 nant physical processes (Figure 12b), and their signs show opposite patterns. At lower level (0~30m), Cond is negative and
265 Vmix is positive, which is the same as their ground characteristics. At upper level (30~200m), Cond is positive and Vmix
266 is negative instead, indicating that fog water is produced by vapor condensation at upper level and then being entrained to
267 ground. The significant positive Cond supports that BLLJ-related moisture advection promotes vapor condensation and fog



268 formation at upper level, and the significant positive V_{mix} may indicate that the upper-level fog favours ground fog for-
269 mation by turbulent exchange of LWC.

270 Figure 13 summarizes the mechanism of fog propagation. During the nighttime, a southerly BLLJ controls the study region,
271 and the jet core intensity is about 10m/s which occurs at about 200m. The ground fog propagates northwestward with the
272 speed of 9.6m/s. The BLLJ favours the fast fog propagation by three possible mechanisms: 1) BLLJ transport sufficient
273 vapor from ocean to inland area. The turbulence strengthened by wind speed shear further moistens the PBL and promotes
274 vapor condensation. This could be the dominant mechanism. 2) BLLJ transports warmer air from ocean to inland area and
275 deepens the inversion layer. The strengthened inversion favours the accumulation of vapor and condensation nuclei. 3) The
276 strong moisture advection could promote the upper-level fog formation in the downstream area, and later it subsides to
277 ground by turbulent exchange of fog droplets. The subsidence of upper-level fog to ground needs to be verified by addi-
278 tional observations.

279 The results could facilitate the understanding of cloud formation and development. Clouds, such as convective clouds, can
280 develop and expand extraordinarily fast under strong synoptic forcing or unstable conditions. Fog can be viewed as a kind
281 of near-surface stratus cloud, which usually forms under stable conditions with weak synoptic forcings. However, as re-
282 vealed in this study, it can also develop and propagates fast under the effect of BLLJ. The quantitative relations between
283 BLLJ and fog fast propagation may have implications on the cloud formation and development mechanism under stable
284 synoptic conditions.

285 4. Conclusions

286 Previous studies have found that the spatial propagation of fog could be rather fast under favourable conditions, and the
287 boundary layer low-level jet (BLLJ) could be a potential reason. In this study, we analyze the fast spatial propagation fea-
288 ture of a large-scale fog event in Jiangsu Province, China by high spatiotemporal resolution ground and satellite observa-
289 tions. The key impact factors and mechanisms of the BLLJ effect on fast spatial propagation are quantitatively revealed by
290 WRF model simulations. Results show that:

291 The fog initials at 22:00 on 20 January 2020 over Jiangsu coastal area, and it reaches the west boundary of Jiangsu at 07:00
292 next day. Satellite retrievals show that the southeast side of fog area varies slightly but the northwest side expands fast,
293 with the maximum propagation speed of 9.6m/s. During the fog period, the ground wind direction is consistent with fog
294 propagation, which favours the vapor transportation from ocean and promotes fog formation. However, the wind speed
295 ($<3\text{m/s}$) is at least one-third less than the fog propagation speed. Therefore, the ground meteorologies are insufficient to
296 explain the fast propagation of fog. The influencing factors and mechanisms need to be investigated by exploring the PBL
297 characteristics through numerical simulations.

298 The WRF model well simulates the temporal variation of meteorologies and reproduces the spatiotemporal evolution of
299 fog area. A BLLJ ($>6\text{m/s}$) exists at the height between 50 and 500m. The jet core occurs at 1000hpa (200m) with the
300 southeasterly winds of 10m/s, which can fit the propagation direction and speed of fog. Therefore, the southeasterly BLLJ



301 is hypothesized to be the cause of fast propagation. BLLJ creates favourable PBL conditions by transporting moisture and
302 warm air from ocean. The moisture advection and the vapor turbulent mixing generated by wind speed shear increase the
303 humidity within PBL, and the propagation of fog area coincides with the movement of high humidity zone (vapor mixing
304 ratio > 4g/kg). The warm advection from ocean deepens inversion layer and additionally favours the accumulation of mois-
305 ture and condensation nuclei. Additionally, it is found that fog could firstly form at upper layer and subsides to ground
306 within 0~20min. The moisture advection is also responsible for the formation of upper-level fog.

307 Sensitive experiments quantitatively reveal the contributions of moisture advection and temperature advection to fog
308 propagation. When moisture (temperature) advection is turned off, the fog area decreases by 62% (50%) and the propaga-
309 tion speed decrease by about 4.6m/s (5.2m/s). Process analysis on fog liquid water content (LWC) further illustrates the
310 mechanism of fog propagation. Condensation (Cond) and LWC turbulent exchange (Vmix) are two important physical
311 processes. At upper level (30~200m), Cond is positive and Vmix is negative. It indicates that BLLJ-related moisture ad-
312 vection significantly promotes condensation and probably favours fog formation at upper level. At ground and lower level
313 (0~30m), Cond is basically negative and Vmix is positive. It indicates that fog droplets at upper level are entrained down-
314 ward by turbulent mixing, leading to the subsequent formation of ground fog. The subsidence of upper-level fog to ground
315 needs to be verified by additional observations.

316 In this study, by combination of observations and simulations, we have revealed the effect of southeasterly BLLJ on fog
317 propagation, and quantified the contributions of BLLJ-related moisture advection and temperature advection to fog propa-
318 gation. Three possible mechanisms are concluded: 1) Moisture advection from ocean promotes vapor condensation in
319 downstream area, which could be the dominant cause; 2) Warm advection from ocean deepens inversion layer and addi-
320 tionally promote vapor accumulation within PBL. 3) The moisture advection probably promotes upper-level fog formation
321 first, and later it subsides to ground by turbulent mixing of fog droplets. The coexistence of fast fog propagation and BLLJ
322 is not a common phenomenon, so finding more cases requires additional work. It should be addressed in future studies in
323 order to deeply understand the relationships between fog propagation and BLLJ under different regions and synoptic con-
324 ditions. Their quantitative relationships could facilitate the understanding of cloud formation and development under stable
325 synoptic conditions, since fog can be viewed as near-surface stratus cloud that can potentially propagate fast under stable
326 conditions.

327

328 *Code and data availability.* Some of the data repositories have been listed in Section 2. The other data, model outputs and
329 codes can be accessed by contacting Duanyang Liu via liuduanyang2001@126.com.

330 *Author contributions.* SY performed the model simulation, data analysis and manuscript writing. HW and DL proposed the
331 idea, supervised this work and revised the manuscript. XL helped the revision of the manuscript. FZ provided and analyzed
332 the observation data.

333 *Competing interests.* The authors declare that they have no conflict of interest.

334 *Acknowledgements.* This work is supported by the Special Project of Innovative Development of CMA (CXFZ2023J022),



335 Open Research Foundation of Jiangsu Marine Meteorology (HYQX2022), Beijige Foundation (BJG202307), Research
336 Foundation of Jiangsu Meteorology Bureau (KM202307), Basic Research Fund of CAMS (2022Y025).

337

338 References

- 339 Andreas, E.L., Claffy, K.J., and Makshtas, A.P.: Low-level atmospheric jets and inversions over the western Weddell Sea,
340 *Boundary Layer Meteorol*, 97(3), 459–486, <https://doi.org/10.1023/A:1002793831076>, 2000.
- 341 Bott, A.: On the influence of the physico-chemical properties of aerosols on the life cycle of radiation fogs, *J. Aerosol Sci*,
342 21(1-2), 1–31, <https://doi.org/10.1007/BF00119960>, 1991.
- 343 Boutle, I., Price, J., Kudzotsa, I., Kokkola, H., and Romakkaniemi, S.: Aerosol-fog interaction and the transition to well-mixed
344 radiation fog, *Atmos. Chem. Phys.*, 18(11), 1–19, <https://doi.org/10.5194/acp-18-7827-2018>, 2017.
- 345 Cermak, J. and Bendix, J.: A novel approach to fog/low stratus detection using Meteosat 8 data, *Atmos. Res.*, 87(3-4), 279–292,
346 <https://doi.org/10.1016/j.atmosres.2007.11.009>, 2008.
- 347 Dhangar, N. G., Lal, D. M., Ghude, S. D., Kulkarni, R., and Rajeevan, M.: On the conditions for onset and development of fog
348 over new delhi: an observational study from the wifex, *Pure Appl. Geophys*, 673, 1-20,
349 <https://doi.org/10.1007/s00024-021-02800-4>, 2021.
- 350 Dupont, J., Haefelin, M., Protat, A., Bouniol, D., Boyouk, N., and Morille, Y.: Stratus–Fog Formation and Dissipation: A 6-Day
351 Case Study, *Boundary-Layer Meteorol*, 143, 207–225, <https://doi.org/10.1007/s10546-012-9699-4>, 2012.
- 352 Di Vittorio, A. V. and Emery, W. J.: An automated, dynamic threshold cloud-masking algorithm for daytime AVHRR images over
353 land, *IEEE Trans. Geosci*, 40, 1682–1694, <https://doi.org/10.1109/TGRS.2002.802455>, 2002.
- 354 Fathalli, M., Lac, C., Burneta, F., and Vié, B.: Fog due to stratus lowering: Experimental and modelling case study, *Q. J. R. Me-*
355 *eteorol*, 148(746), 2299–2324. <https://doi.org/10.1002/qj.4304>, 2022.
- 356 Gao, S., Lin, H., Shen, B., and Fu, G.: A heavy sea fog event over the Yellow Sea in March 2005: Analysis and numerical mod-
357 eling, *Adv Atmos Sci*, 24, 65-81, <https://doi.org/10.1007/s00376-007-0065-2>, 2007.
- 358 Gao, Y., Liu, D., Yan, S., Zhou, W., Wang, H., Zu, F., Mei, Q., Yi, C., and Sheng, Y.: Influence of sea-land breeze on formation
359 and dissipation of severe dense fog and its explosive enhancement in the Yellow Sea Coastal Area, *Sci. China Earth Sci.*,
360 2023. (accepted; under translation into English)
- 361 Gulpepe, I., Tardif, R., Michaelides, S. C., Cermak, J., Bott, A., Bendix, J., Muller, M. D., et al.: Fog research: a review of past
362 achievements and future perspectives, *Pure Appl. Geophys*, 164, 1121–1159, <https://doi.org/10.1007/s00024-007-0211-x>,
363 2007.
- 364 Haefelin, M., Bergot, T., Elias, T., Tardif, R., Carrer, D., Chazette, P., and Zhang, X.: PARISFOG: Shedding new light on fog
365 physical processes, *Bull Am Meteorol Soc*, 91(6), 767-783, <https://doi.org/10.1175/2009bams2671.1>, 2010.
- 366 Jia, X., Quan, J., Zheng, Z., Liu, X., Liu, Q., He, H., and Liu, Y.: Impacts of anthropogenic aerosols on fog in North China Plain,
367 *J. Geophys. Res.-Atmos.*, 124, 252–265, <https://doi.org/10.1029/2018jd029437>, 2018.
- 368 Jiao, S., Zhu, C., Zhu, Y., Yuan, C., Zu, F., and Sun, K.: A discussion on the reason for a rare persistent heavy fog event in Jiang-
369 su Province, *Acta Meteorol. Sin.*, 74, 200–212, <https://doi.org/10.11676/qxxb2016.015>, 2016.
- 370 Koračin, D., Dorman, C. E., Lewis, J. M., Hudson, J. G., Wilcox, E. M., and Torregrosa, A.: Marine fog: A review, *Atmos. Res.*,
371 143, 142-175, <https://doi.org/10.1016/j.atmosres.2013.12.012>, 2014.
- 372 Korb, G. and Zdunkowski, W.: Distribution of radiative energy in ground fog, *Tellus*, 22(3), 298-320,
373 <https://doi.org/10.3402/tellusa.v22i3.10223>, 1970.
- 374 Kraus, H., Malcher, J., and Schaller, E.: A nocturnal low level jet during PUKK, *Boundary Layer Meteorol*, 31, 187-195,
375 <https://doi.org/10.1007/BF00121177>, 1985.
- 376 Kunkel, B. A.: Parameterization of Droplet Terminal Velocity and Extinction Coefficient in Fog Models, *J. Appl. Meteorol*, 23(1),
377 34–41, [https://doi.org/10.1175/1520-0450\(1984\)023<0034:PODTVA>2.0.CO;2](https://doi.org/10.1175/1520-0450(1984)023<0034:PODTVA>2.0.CO;2), 1983.
- 378 Li, P. and Fu, G.: The Formation Mechanism of a Spring Sea Fog Event over the Yellow Sea Associated with a Low-Level Jet,
379 *Weather and Forecasting*, 27(6), 1538-1553, <https://doi.org/10.1175/WAF-D-11-00152.1>, 2012.



- 380 Li, Z. H., Liu, D. Y., Yang, J.: The microphysical processes and macroscopic conditions of the radiation fog droplet spectrum
381 broadening, *Chinese J. Atmospheric Sci.*, 35, 41–54, <https://doi.org/10.3878/j.issn.1006-9895.2011.01.04>, 2011. (in Chinese)
- 382 Li, Z., Liu, D., Yan, W., Wang, H., Zhu, C., Zhu, Y., and Zu, F.: Dense fog burst reinforcement over Eastern China: A review,
383 *Atmos. Res.*, 230(D19), 104639, <https://doi.org/10.1016/j.atmosres.2019.104639>, 2019.
- 384 Liu, D., Yang, J., Niu, S., and Li, Z.: On the Evolution and Structure of a Radiation Fog Event in Nanjing, *Adv Atmos Sci*, 28(1),
385 223-237, <https://doi.org/10.1007/s00376-010-0017-0>, 2011.
- 386 Liu, D. Y., Niu, S. J., Yang, J., Zhao L., Lv, J., and Lu, C.: Summary of a 4-year fog field study in Northern Nanjing, part 1: fog
387 boundary layer, *Pure Appl. Geophys.*, 169, 809–819, <https://doi.org/10.1007/s00024-011-0343-x>, 2012.
- 388 Liu, D., Yan, W., Yang, J., Pu, M., Niu, S., Li, Z.: A Study of the Physical Processes of an Advection Fog Boundary Layer,
389 *Boundary Layer Meteorol*, 158(1), 125-138, <https://doi.org/10.1007/s10546-015-0076-y>, 2016.
- 390 Liu, D., Li, Z., Yan, W., and Li, Y.: Advances in fog microphysics research in China, *Asia Pac J Atmos Sci*, 53(1), 131–148,
391 <https://doi.org/10.1007/s13143-016-0028-6>, 2017.
- 392 Liu, Q., Wang, Z. Y., Wu, B. G., Liu, J. L., and Gultepe, I.: Microphysics of fog bursting in polluted urban air, *Atmospheric En-*
393 *viron.*, 10, 118357, <https://doi.org/10.1016/j.atmosenv.2021.118357>, 2021.
- 394 Nakanishi, M.: Large-eddy simulation of radiation fog. *Boundary Layer Meteorol*, 94, 461-493,
395 <https://doi.org/10.1023/A:1002490423389>, 2000.
- 396 Pleim, J. E., Gilliam, R.: An indirect data assimilation scheme for deep soil temperature in the Pleim-Xiu land surface model, *J.*
397 *Appl. Meteorol*, 48, 1362-1376, <https://doi.org/10.1175/2009JAMC2053.1>, 2009.
- 398 Pu, M. J., Zhang, G. Z., Yan, W. L., and Li, Z. H.: Features of a rare advection-radiation fog event, *Sci. China Earth Sci.*, 51(7),
399 1044–1052, <https://doi.org/10.1007/s11430-008-0071-y>, 2008.
- 400 Quan, J., Liu, Y., Jia, X., Liu, L., Dou, Y., Xin, J., and Seinfeld, J. H.: Anthropogenic aerosols prolong fog lifetime in China, *En-*
401 *viron. Res. Lett.*, 16(4), 044048, <https://doi.org/10.1088/1748-9326/abef32>, 2021.
- 402 Schwenkel, J. and Maronga, B.: Large-eddy simulation of radiation fog with comprehensive two-moment bulk microphysics:
403 impact of different aerosol activation and condensation parameterizations, *Atmos. Chem. Phys.*, 19(10), 1-23,
404 <https://doi.org/10.5194/acp-19-7165-2019>, 2018.
- 405 Shen, P., Liu, D., Gultep, I., Lin, H., Cai, N., and Cao, S.: Boundary layer features of one winter fog in the Yangtze River Delta,
406 China, *Pure Appl. Geophys.*, 179(9), 3463-3480, <https://doi.org/10.1007/s00024-022-03119-4>, 2022.
- 407 Steeneveld, G. J., Ronda, R. J., and Holtslag, A. A. M.: The Challenge of Forecasting the Onset and Development of Radiation
408 Fog Using Mesoscale Atmospheric Models, *Boundary Layer Meteorol*, 154(2), 265–289,
409 <https://doi.org/10.1007/s10546-014-9973-8>, 2014.
- 410 Sukoriansky, S., Galperin, B., Perov, V.: Application of a new spectral model of stratified turbulence to the atmospheric boundary
411 layer over sea ice, *Boundary Layer Meteorol*, 117, 231–257, <https://doi.org/10.1007/s10546-004-6848-4>, 2005.
- 412 Tian, M., Wu, B., Huang, H., Zhang, H., Zhang, W., and Wang, Z.: Impact of water vapor transfer on a Circum-Bohai-Sea heavy
413 fog Observation and numerical simulation, *Atmos. Res.*, 229, 1-22, <https://doi.org/10.1016/j.atmosres.2019.06.008>, 2019.
- 414 van der Velde, I. R., Steeneveld, G. J., Wichers Schreur, B. G. J., and Holtslag, A. A. M.: Modeling and Forecasting the Onset
415 and Duration of Severe Radiation Fog under Frost Conditions, *Mon Weather Rev*, 138(11), 4237–4253,
416 <https://doi.org/10.1175/2010mwr3427.1>, 2010.
- 417 Wang, H., Zhang, Z., Liu, D., Zhu, Y., Zhang, X., and Yuan, C.: Study on a Large-Scale Persistent Strong Dense Fog Event in
418 Central and Eastern China, *Adv. Meteorol*, 4, 1–15, <https://doi.org/10.1155/2020/8872334>, 2020.
- 419 Wang, Y., Lu, C., Niu, S., Lv, J., Jia, X., Xu, X., et al.: Diverse dispersion effects and parameterization of relative dispersion in
420 urban fog in eastern China, *J. Geophys. Res.-Atmos.*, 128, e2022JD037514, <https://doi.org/10.1029/2022JD037514>, 2023.
- 421 Wei, W., Zhang, H. S., Ye, X. X.: Comparison of low-level jets along the north coast of China in summer, *J. Geophys.*
422 *Res.-Atmos.*, 119(16), 9692–9706, <https://doi.org/10.1002/2014JD021476>, 2014.
- 423 Wobrock, W., Schell, D., Maser, R., Kessel, M., Jaeschke, W., Fuzzi, S., and Bendix, J.: Meteorological characteristics of the Po
424 Valley fog, *Tellus B*, 44(5), 469-488, <https://doi.org/10.3402/tellusb.v44i5.15562>, 1992.
- 425 Wu, B., Li, Z., Ju, T., and Zhang, H.: Characteristics of Low-level jets during 2015–2016 and the effect on fog in Tianjin, *Atmos.*
426 *Res.*, 245, 105102, <https://doi.org/10.1016/j.atmosres.2020.105102>, 2020.



- 427 Yan, S., Zhu, B., Huang, Y., Zhu, J., Kang, H., Lu, C., and Zhu, T.: To what extents do urbanization and air pollution affect fog?,
428 *Atmos. Chem. Phys.*, 20(9), 5559–5572, <https://doi.org/10.5194/acp-20-5559-2020>, 2020.
- 429 Yang, Y., Hu, X.-M., Gao, S., and Wang, Y.: Sensitivity of WRF simulations with the YSU PBL scheme to the lowest model level
430 height for a sea fog event over the Yellow Sea, *Atmos. Res.*, 215, 253–267, <https://doi.org/10.1016/j.atmosres.2018.09.004>,
431 2019.
- 432 Ye, X., Wu, B., and Zhang, H.: The turbulent structure and transport in fog layers observed over the Tianjin area, *Atmos. Res.*,
433 153, 217-234, <https://doi.org/10.1016/j.atmosres.2014.08.003>, 2015.
- 434 Zhang, G., Bian, L., Wang, J., Yang, Y., Yao, W., and Xu, X.: The boundary layer characteristics in the heavy fog formation pro-
435 cess over Beijing and its adjacent areas, *Sci. China Earth Sci.*, 48, 88-101, <https://doi.org/10.1360/05yd0029>, 2005.
- 436 Zhu, Y., Zhu, C., Zu, F., Wang, H., Liu Q., Qi, M., and Wang, Y.: A persistent fog event involving heavy pollutants in Yancheng
437 area of Jiangsu Province, *Adv. Meteorol.*, 2018, 2512138, <https://doi.org/10.1155/2018/2512138>, 2018.
- 438 Zhu, Y., Li, Z., Zu, F., Wang, H., Liu, Q., Qi, M., and Wang, Y.: The propagation of fog and its related pollutants in the Central
439 and Eastern China in winter, *Atmos. Res.*, 265, 105914, <https://doi.org/10.1016/j.atmosres.2021.105914>, 2022.
- 440



441 Table 1. Model parameterization schemes and sensitive experiments

Physical scheme	Option
Boundary layer	QNSE
Microphysics	Lin double moment
Longwave radiation	RRTM
Shortwave radiation	Goddard
Land surface	Pleim-Xiu
Cumulus	Grell-3D
Grid nudging	Off
Observation nudging	Off
Experiment	Description
Base	The base condition
Tadv0	Turning off temperature advection
QvAdv0	Turning off water vapor advection
QcAdv0	Turning off fog water advection
NoAdv	Turning off all advections above

442

443 Table 2. The times when visibility reaches 1000m, 500m and 200m at three representative stations. (DF:Dafeng,
444 BY:Baoying, SH:Sihong).

Station	Location	Formation (Vis=1000m)		Vis=500m		Vis=200m	
		Time	Wind	Time	Wind	Time	Wind
DF	120.48°E,33.20°N	19:45	1.3m/s, E	22:55	1.2m/s, E	23:45	1.3m/s, E
BY	119.30°E,33.23°N	01:25	1.2m/s, ESE	03:15	1.4m/s, ESE	03:45	1.3m/s, SE
SH	118.22°E,33.48°N	04:50	1.6m/s, ESE	06:10	1.3m/s, ESE	07:15	2.4m/s, ESE
	Distance (km)	Time difference (h)		Time difference (h)		Time difference (h)	
DF-BY	110	4.7		4.3		4.0	
BY-SH	105	3.4		2.9		3.5	

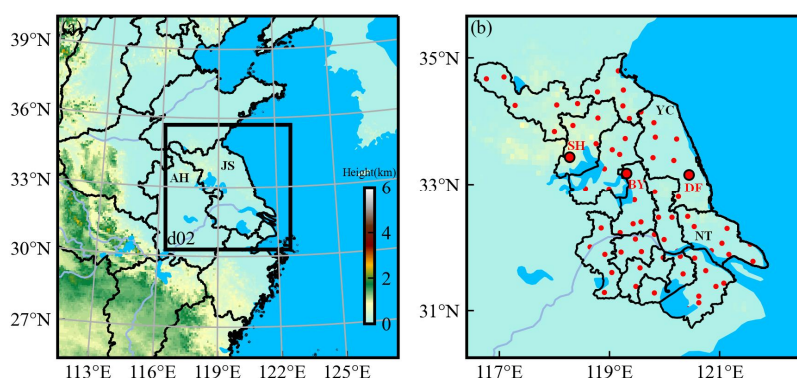
445

446

447



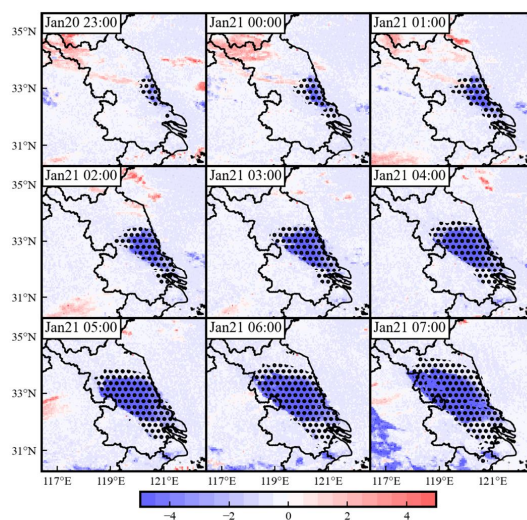
448



449

450 Figure 1. The parent and nest model domain. The shaded color is terrain height. The red points are automatic weather stations
451 in Jiangsu, China; and the three larger points are Sihong (SH), Baoying (BY), and Dafeng (DF) stations. The black labels are
452 some province or city names. (JS:Jiangsu Province; AH:Anhui Province; YC:Yanchen; NT:Nantong).

453

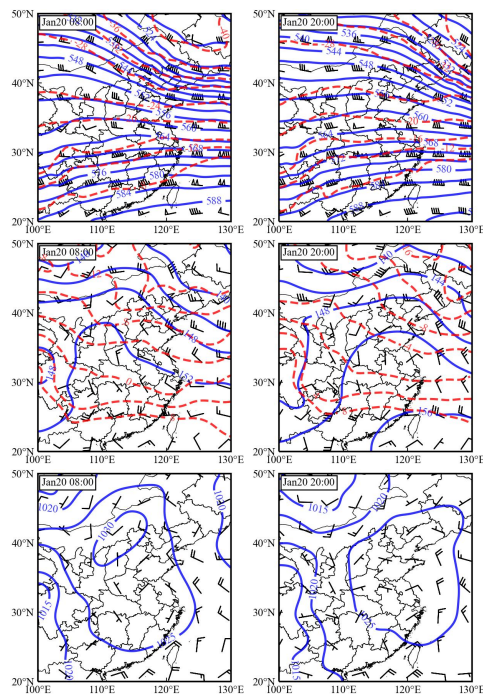


454

455 Figure 2. The spatial evolution of fog. The black dots are simulated fog areas. The shaded colors are satellite observed bright-
456 ness temperature difference ($3.9\mu\text{m}$ minus $11.2\mu\text{m}$), where the blue colors (smaller than -2 K) indicate the fog areas.

457

458



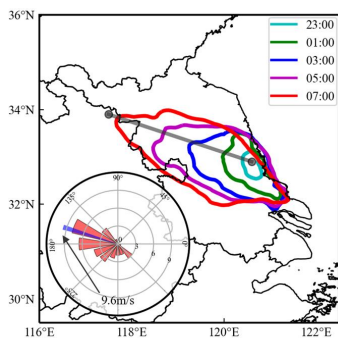
459

460 Figure 3. The synoptic background of 500hpa (first row), 850hpa (second row) and surface (third row) at 08:00 and 20:00 on
461 20 January 2020.

462



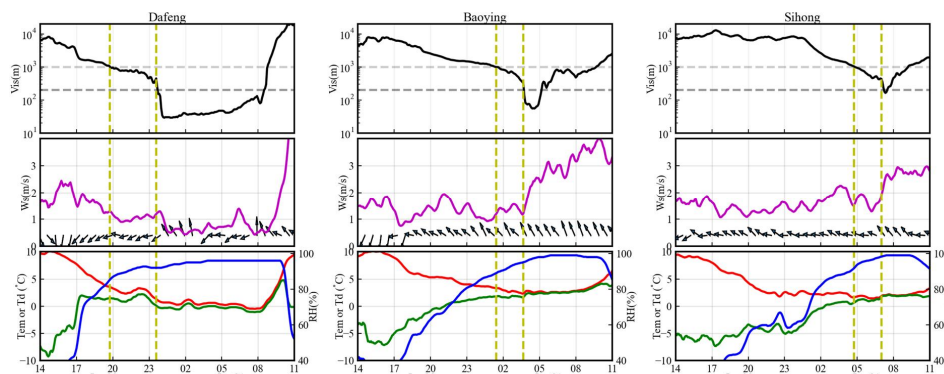
463



464

465 Figure 4. The colored curves are the fog boundaries (satellite retrievals) from 23:00 on 20 January to 07:00 next day every 2
 466 hours. The gray straight line indicates the fog propagation direction, and the vertical features of meteorologies at this line will be
 467 analyzed in Figures 7, 8, and 9. The lower-left polar plot is the fog propagation speed at 16 directions (22.5° interval), and the
 468 narrow blue bar highlights the maximum propagation speed (9.6m/s) occurring at 160° direction (north-northwest).

469



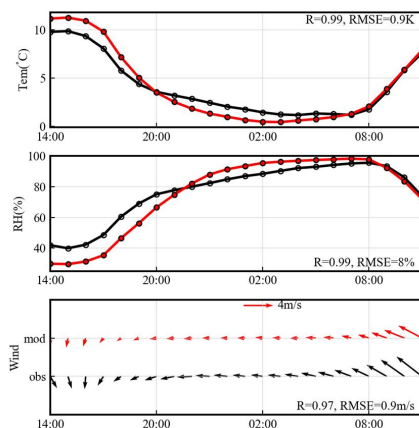
470

471 Figure 5. The temporal variation of ground visibility (Vis; black line), wind speed (Ws; pink line), wind direction (vectors),
 472 temperature (Tem; red line), dew point (Td; green line) and relative humidity (RH; blue line) at Dafeng, Baoying, and Sihong
 473 stations. The horizontal dashed lines are visibilities of 1000m and 200m. The vertical dashed lines mark the times of fog for-
 474 mation and visibility burst dropping.

475



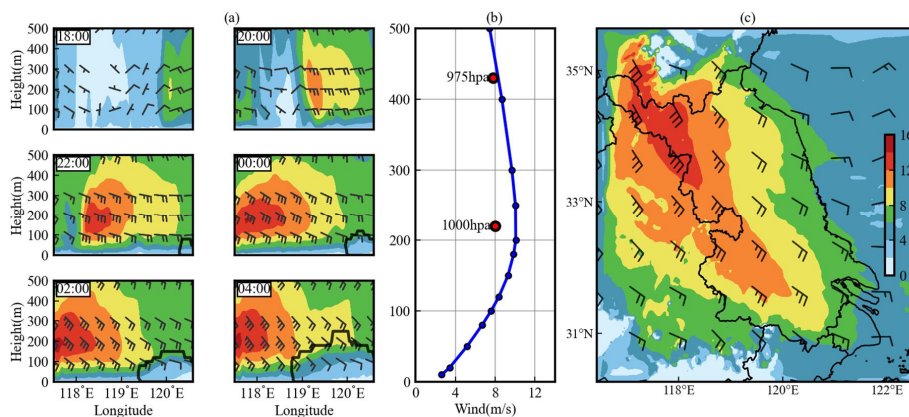
476



477

478 Figure 6. The model performance on 2m Temperature (Tem), 2m Relative humidity (RH) and 10m wind speed and direction.
479 The red color is simulation and black color is observation. The time is from 14:00 on 20 January 2020 to 11:00 next day.

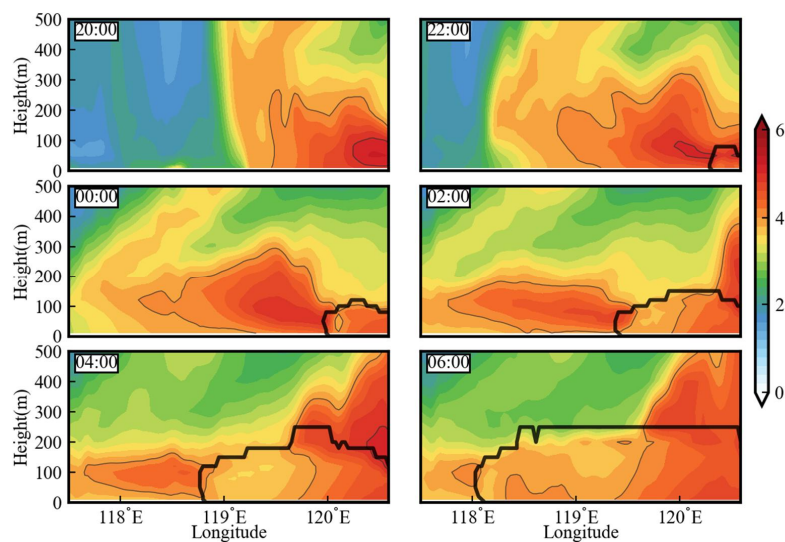
480



481

482 Figure 7. (a) The height-longitude variation of horizontal wind direction (vectors) and wind speed (shaded colors) at the cross-
483 ing line in Figure 4. The lower-right black polygons are the fog area. The times are from 18:00 on 20 January to 04:00 next day.
484 (b) The averaged wind speed profile at the crossing line during 23:00-07:00. The two red points are the wind speed calculated
485 from ERA5 reanalysis. (c) The averaged wind direction (vectors) and wind speed (shaded colors) at 1000hpa during
486 23:00-07:00.

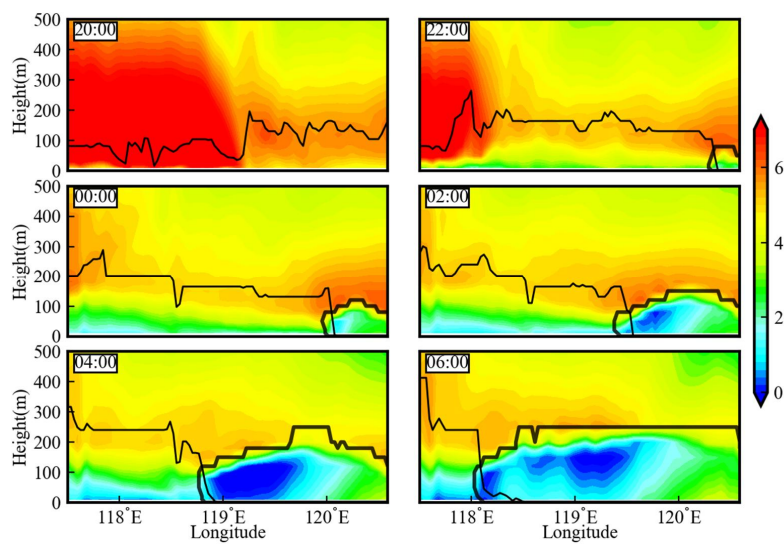
487



488

489 Figure 8. The height-longitude distribution of water vapor mixing ratio (g/kg) at the crossing line in Figure 4. The deep black
490 polygons are the fog area. The light black lines are the region of water vapor mixing ratio larger than 4g/kg. The times are from
491 20:00 on 20 January to 06:00 next day.

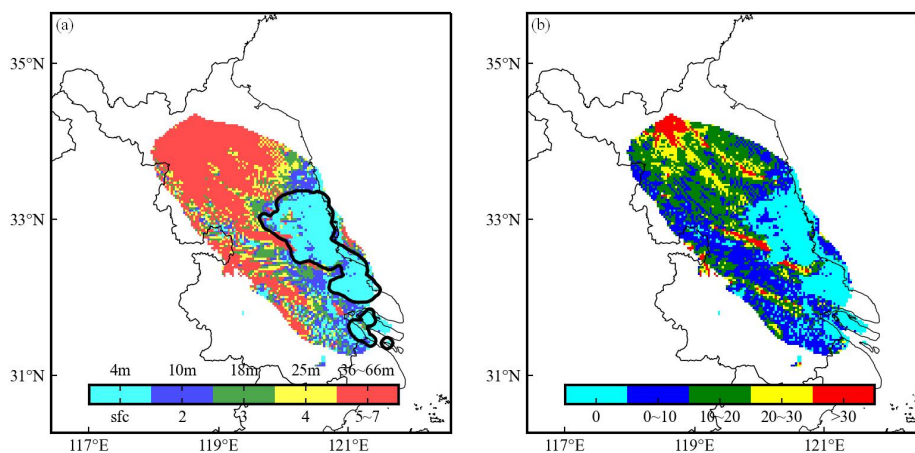
492



493

494 Figure 9. Same as the previous figure, but for the temperature. The bold black polygons are the fog area. The thin black lines
495 are the top of inversion layer.

496

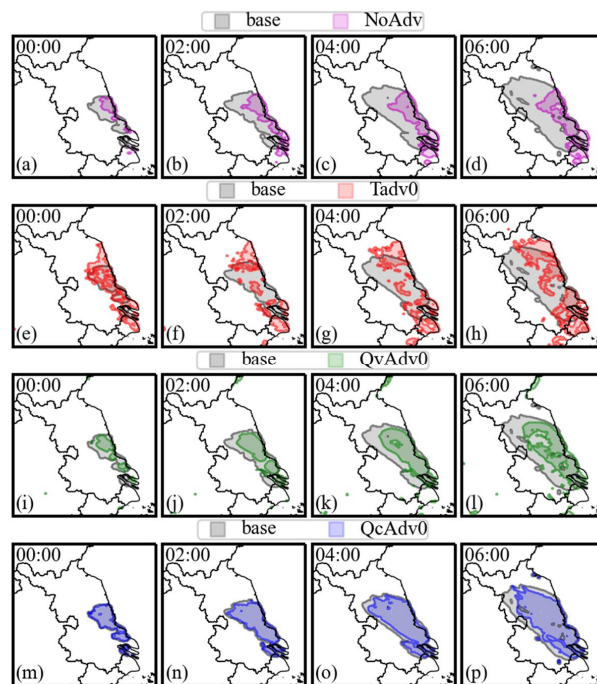


497

498 Figure 10. (a) The height (shaded color) at which fog firstly forms. The black contours are the ground fog areas at 00:00 on 21
499 January 2020. The colorbar represents the model level and the corresponding height above surface. For example, the cyan colors
500 indicate that fog firstly forms at the surface level with the corresponding height of about 4m. The red colors indicate that fog
501 firstly forms at the 5th to 7th model level with the corresponding height of about 36~66m. (b) The time differences between
502 ground fog formation and upper-level fog formation. For example, the cyan colors indicate that fog firstly forms at ground. The
503 blue colors indicate that the ground fog forms 0~10min later than the upper-level fog formation.
504
505



506

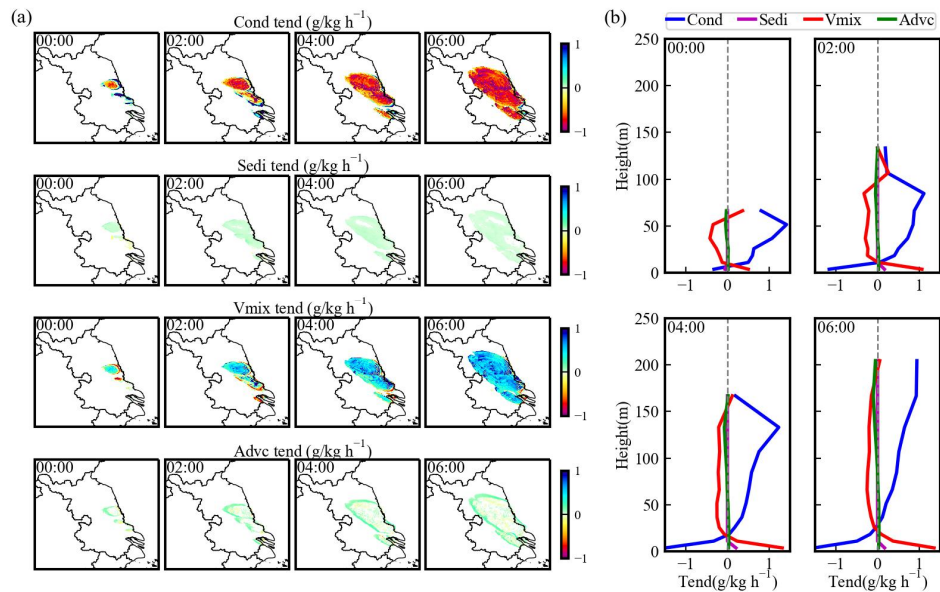


507

508 Figure 11. The temporal variation of ground fog area under different experiments from 00:00 to 06:00 on 21 January. The black
509 color is the base experiment. The Tadv0 (red), QvAdv0 (green) and QcAdv0 (blue) are the experiments turning off temperature
510 advection, moisture advection and fog water advection, respectively. The NoAdv (pink) is the experiment turning off all of the
511 above advectons.
512



513

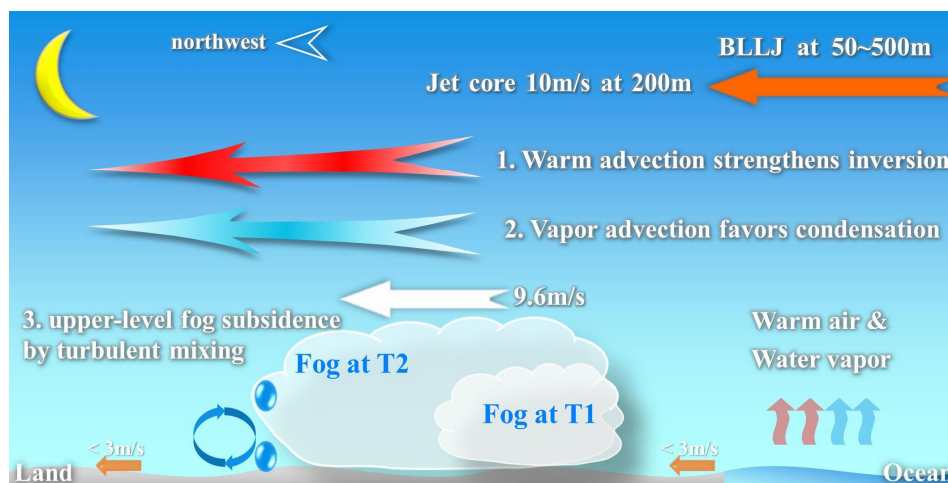


514

515 Figure 12. (a) The spatial distribution of the four process tendencies contributing to LWC variation at ground level. (b) The
 516 vertical profiles of the process tendencies averaged in fog area. The times are from 00:00 to 06:00 on 21 January.
 517 (Cond:condensation or evaporation; Sedi:sedimentation; Vmix:turbulent exchange; Advc:horizontal and vertical advection).
 518



519



520

521 Figure 13. The concept diagram of fog propagation. The ground wind speed (short orange arrows) is generally less than 3m/s.
522 A southeasterly BLLJ exists at the height from 50 to 500m, and the jet core intensity is 10m/s at 200m (the long orange arrow).
523 The updraft arrows represent the warm and wet air from ocean. The two cloud shapes are fog areas at two adjacent times, and the
524 white arrow indicates the fog propagation speed (9.6m/s). The fog propagation is probably caused by three approaches: 1) Moisture
525 advection from ocean promotes vapor condensation in the downstream area, which could be the dominant cause (the blue
526 fancy arrow); 2) Warm advection from ocean deepens inversion layer and additionally promotes vapor accumulation within PBL
527 (the red fancy arrow); 3) The moisture advection probably result in the upper-level fog formation, and later it subsides to ground
528 by turbulent mixing of fog droplets (the blue water drops and circular arrows).